

KINETIC MODEL OF THE ELECTRON AND ION TRANSPORT IN HALL THRUSTERS

I. Levchenko^a and M. Keidar^b

^aNational Aerospace University, Kharkov, Ukraine. E-mail: iglev@ukr.net

^bDepartment of Aerospace Engineering, University of Michigan, Ann Arbor, MI 48109.
E-mail: keidar@engin.umich.edu

In this paper a particle model of the plasma processes in Hall thruster channel is presented. A hybrid model is developed in which the atom ensemble is described in 2D monochrome (2D0V) approximation, ion ensemble - in 2D2V, and electron ensemble - in 2D Maxwell distribution function approximations. This model is used for studying the 2D electron, atom and ion distributions, as well as for studying electron and ion current profiles in the acceleration channel. Quasi-neutrality assumption is relaxed in this model. The influence of the secondary electron emission coefficient of the dielectric walls on the above parameters was addressed. Specifically the effects of the low-voltage ions flux to the charged ceramic walls, as well as ion recombination on the walls are taken into account. The numerical calculations show that this model predicts the main thruster parameters and allow studying of the plasma characteristics in the channel. In particular, the model shows the well-shaped acceleration zone with strong electrical field reaching 30000 V/m, the electrical field peak coinciding with the magnetic field maximum. The low-voltage ion flux to the thruster walls has a maximum located between the anode and ionization zone, closer to the ionization zone.

I. INTRODUCTION

The Hall thruster, sometimes named the stationary plasma thruster, is the most promising type of spacecraft low-thrust devices. The main distinguishing feature of this thruster is high density of thrust current that is not limited by the space charge in the acceleration channel. This provides the high efficiency and small geometrical dimensions of the device, as compared with the ion thrusters. The cross-field transport in the electrical field (E) and magnetic field (B), as well as closed electron drift are the characteristic features of the Hall thruster physics¹. At present, two main versions of the Hall thrusters are being investigated, namely the thrusters with ceramic wall, or stationary plasma thrusters, and thrusters with metal walls, sometimes called the thrusters with anode layer². In the present paper we examine the processes in a stationary plasma thrusters paying special attention to the near-wall processes and spatial distribution of the plasma parameters in the thruster channel.

The processes in Hall thrusters are being investigated for several decades^{3,4} but some questions are still opened. The problem of the anomalous electron drift across the magnetic field in Hall thrusters was firstly explained by A. Morozov in terms of near-wall conductivity⁵. Subsequent studies used the assumptions about the Bohm diffusion⁶ and near-wall conductivity⁷. It was concluded that in principal both effects must be taken into consideration while analyzing the electron transport⁸. In particular, interesting effects related to electron transport were obtained when segmented electrodes are placed inside of the dielectric channel^{9,10}. However the question about the main mechanism of electron transport in the Hall thruster channel remains open. In this paper the above electron transport mechanisms were used together with the assumption about the ion flux neutralization on the charged ceramic walls of the thruster channel¹¹. For studying the above processes two general approaches are mainly used, namely the hydrodynamic approach and particle method. In this paper we give a preference to the second way, which is much more time – consuming with respect to the computation time, but allows to analyze some additional feature such as spatial ion and electron energy distribution in thruster channel. Taking into account that the electron relaxation time is small enough, we developed a hybrid model that uses the particle method for heavy species (ions and atoms) and fluid approximation for electrons.

In this paper the model is described in some details and results of numerical study of the transport and ionization processes in Hall thruster channel are presented. The electron collisions with dielectric walls, classical electron mobility in crossed fields, and Bohm diffusion are taken into account when electron transport is considered across the magnetic field. The electron ensemble energy was calculated taking into account the energy losses in ionization collisions and inelastic collisions with channel walls. We make the special emphasis on near-wall processes related to the electron drift across the magnetic field, electron current distribution, and electrical field distribution in the acceleration channel.

II. MODEL

A. General model considerations

1. We used 2D approximation for ion, electron, and neutral components in the channel. The ion transport was described with 2D2V Vlasov equation, neutral flow was described with the 2D transport equation, and electron transport was described with 2D assuming Maxwell energy distribution function. These assumptions provide some computational problems but allow calculation of 2D profiles for all components.
2. In this model we did not use the quasineutrality assumption, so the electrical field is calculated from Poisson equation.
3. Electron mobility was calculated from classical atom-electron, Bohm, and electron-wall collisions. The ion-electron and electron-electron collisions were neglected.
4. In this work we used an assumption about the Maxwellian distribution function for electrons.

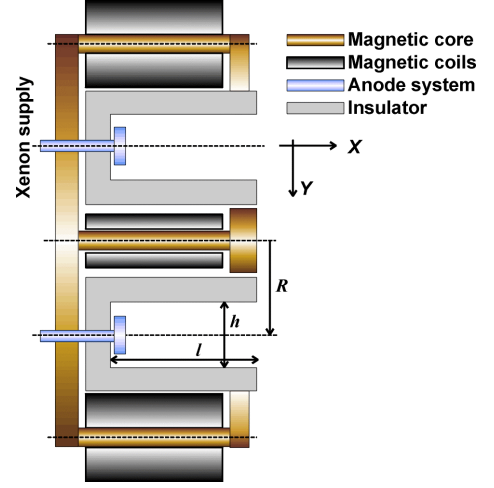


Fig. 1. Scheme of a Hall thruster.
Cathode is not shown.

B. Thruster geometry and main parameters

General scheme of a Hall thruster is shown in Fig. 1. In this work we used the Hall thruster geometry close to that of SPT-100¹²: mean channel radius $R=40$ mm, channel length $l=30$ mm, and channel width $h=20$ mm. The magnetic field has a bell-shaped form with a maximum value of about 0.022 T inside the channel ($\approx 0.85 l$), and 0.002 T at the anode. The xenon mass flow rate was varied from 3 to 5 mg/s. The channel wall material was characterized by the secondary electron mission coefficient k_s that varies from 0.75 to 0.95, that corresponding to the boron nitride usually used in Hall thrusters. The xenon was assumed to be uniformly injected in the anode plane. The external voltage of 300 V was applied across the channel between the anode and exit plane. Ceramic walls were assumed to be perfectly smooth, i.e. the influence of wall roughness to the electron-wall collision process was neglected.

C. Neutral component

The propellant (xenon) is injected into the thruster channel at the anode plane at a room temperature of 300 °C. In the present model we assume that the xenon flow velocity does not change along the channel, and the initial velocity is maintained:

$$V_a = \sqrt{\frac{3kT}{m_a}} \quad (1)$$

Where m_a is the atom mass, k is Boltzmann constant, and T is temperature. The atom density near anode is calculated for the given mass flow m_r and is uniform along the channel width:

$$n_{aa} = \frac{m_r}{V_a S m_a} \quad (2)$$

Where S is the channel (anode) cross-section, m_r is the atom mass flow rate, m_a is the xenon atom mass.

Xenon atom density in the chamber is described by the transport equation:

$$\frac{\partial n_a}{\partial t} + V_a \frac{\partial n_a}{\partial x} = -\mu_i \quad (3)$$

Where μ_i is the xenon ionisation rate that in general is calculated as:

$$\mu_i = \int_0^{\infty} \sigma_i(V_e) n_a V_e f(V_e) dV_e \quad (4)$$

where σ_i is the atom – electron ionization cross-section, V_e is the electron velocity, and $f(V_e)$ is the electron velocity distribution function. It was shown that in Hall thrusters the electron distribution function could be two-humped¹³. In general this experimental data may be used for increasing accuracy. In the presented here results we used the assumption about Maxwell electron distribution function with a view to accelerate the calculations. In this approximation the equation (4) may be written as:

$$\mu_i = n_a \cdot n_e \cdot \sigma_i \cdot V_e \quad (5)$$

Left boundary condition for equation (3) may be written in the form:

$$n_a |_{x=0} = n_{aa} \quad (6)$$

where n_{aa} is calculated from equation (2). That means the xenon inflow from anode with mass flow rate m_r .

Right boundary condition for equation (3) is the xenon free outflow.

D. Ion component

The ion component is described with the ion Vlasov equation:

$$m_i V_i \frac{\partial f_i}{\partial x} + e \frac{\partial \varphi(x, y)}{\partial x} \frac{\partial f_i}{\partial V_i} = \frac{\mu_i}{V_0} \quad (7)$$

Where V_i is the ion velocity, μ_i is the ionization rate, m_i is the ion mass, and f_i is the ion distribution function. In this equation the assumption is used about ion production with velocity equal to atom velocity V_0 .

We did not use the quasineutrality assumption in this model so the potential $\varphi(x, y)$ is calculated from the Poisson equation:

$$\nabla^2 \varphi = - \frac{\rho_e}{\epsilon_0} \quad (8)$$

where φ is the electric potential, ρ_e is the electrical charge density, and ϵ_0 is the dielectric constant. The ion production rate is equal to the xenon atom ionization rate, i.e.

$$\mu_i = n_a \cdot n_e \cdot \sigma_i \cdot V_e \quad (9)$$

Total ion current in the channel (as a function of coordinate x along the channel) is calculated:

$$J_i(x) = e \int_S \int_{V_i} f_i V_i dV_i dS \quad (10)$$

where V_i is the ion velocity, S is the channel cross-section area.

The ion density is calculated by integrating the ion distribution function:

$$n_i(x, y) = \int_S f_i dV_i \quad (11)$$

And the total thrust can be found by integrating in the channel exit plane:

$$F = m_i \int_S \int_{V_i} f_i V_i^2 dV_i dS \quad (12)$$

Where S is the channel cross-section area.

E. Electron component

According to the above conditions, the electron component is described as collisionless fluid that flows from the exit plane to anode across the magnetic field that has only radial component. (axial components are neglected). Under this assumption the electron density can be calculated from the transport equation taking into account the electron mobility across the magnetic field and electron flux due to ionization:

$$\frac{\partial n_e}{\partial t} + \frac{\partial(n_e V)}{\partial x} + \frac{\partial(n_e V)}{\partial y} = -\mu_i \quad (13)$$

The 2D electron energy distribution over the channel length and width was calculated using a system of two equations describing the energy diffusion. The equation of energy diffusion in axial direction (along X axis) reads:

$$\mu_e E_x \left[\frac{\partial \mathcal{E}_e}{\partial x} + E_x e \right] = \psi_e \quad (14)$$

Where μ_e is the electron mobility across magnetic field, ψ_e is the energy loss rate calculated as energy losses due to ionization with rate μ_i and wall collisions that produce secondary electrons. The equation of energy diffusion in radial direction (Y axis) can be written in similar form with use of the classical electron mobility due to collisions along the magnetic field. The system of two energy diffusion equations allow calculation of the 2D electron energy distribution in thruster channel.

The electron mobility μ_e across the magnetic field is the most complicated question of the electron anomalous conductivity in the Hall thrusters. In this model we use the electron mobility in the form:

$$\mu_e = \frac{e}{m_e \nu_e} \frac{1}{1 + \bar{\omega}^2} \quad (15)$$

Where $\bar{\omega} = \frac{\omega}{\nu_e} = \frac{eB}{m_e \nu_e}$, ω is the cyclotron frequency, and ν_e is the total electron collision frequency.

The total electron collision frequency is calculated as:

$$\nu_e = \nu_{ea} + \nu_i + \nu_B + \nu_{ew} \quad (16)$$

Where ν_{ea} is the electron – atom elastic collision frequency, ν_i is the electron – atom ionization collision frequency, ν_B is the anomalous Bohm diffusion collision frequency, and ν_{ew} is the electron – wall collision frequency. The electron – atom elastic collision frequency and electron – atom ionization collision frequency are calculated as follows:

$$\nu_{ea} = n_a \cdot V_e \cdot \sigma_{ea}(\mathcal{E}) \quad (17)$$

$$\nu_i = n_a \cdot V_e \cdot \sigma_{ei}(\mathcal{E}) \quad (18)$$

where $\sigma_{ea}(\mathcal{E})$ is the collision cross-section that depends on the electron energy, and V_e is the mean electron velocity.

The experiments show that the use of only classical collisions cannot provide good agreement with the experiments, and the real electron current in Hall thrusters exceeds significantly the value that can be calculated from the equation (16). To provide the agreement, electron-wall collisions and the anomalous Bohm diffusion collision are often involved. In the model we will use both these effects.

The Bohm collisions are calculated:

$$\nu_B = \omega_e / 16 \quad (19)$$

where 16 is the empirical coefficient. It should be noted that this value is rather excessive, at least in relation to the Hall thrusters, and the coefficient of 50...100 is recommended⁸.

Electron – wall collision frequency corresponds to the concept of near-wall conductivity, and can be calculated from the following equation:

$$\nu_{ew}(x) = \frac{V_e(x)}{2h} e^{-\frac{eU_w}{kT_e}} \quad (20)$$

Where V_e is the electron velocity near the channel wall, i.e. on the sheath border, and U_w is the channel wall potential. The wall potential is determined mainly by the electron influx along the magnetic field lines and depends strongly on the secondary electron emission coefficient, which reduces the U_w due to secondary electron emission from the wall material and hence reduces the total wall charge. In our case when the SPT thruster with ceramic walls is considered the surface current along the channel wall is impossible. This leads to the wall potential dependence on the distance along channel length, and wall potential can be calculated as follows:

$$U_w(x) = \frac{kT_e(x, y=0)}{2e} \ln \left((1 - k_s) \sqrt{\frac{m_i}{m_e}} \right) \quad (21)$$

where $U_w(x)$ – wall potential in the point (X), $T_e(x, y=0)$ is the electron temperature near channel wall, and k_s is the secondary electron emission coefficient.

The secondary electron emission coefficient k_s is often assumed in the range of 0.75 to 0.95 for boron nitride walls. Another way is to calculate this value as a function of electron energy²: $k_s = a \cdot \varepsilon^b$, with $a = 0.141$ and $b = 0.567$ for boron nitride, and ε is the electron energy near channel wall, eV. In our model we use both approaches for calculation k_s .

The electron current to the wall for general case of electron distribution function $f(\varepsilon)$ will be calculated:

$$J_w(x) = e v_{ew}(x) \int_{U_w}^{\infty} f(\varepsilon) \cdot d\varepsilon \quad (22)$$

The axial electron current density was calculated in terms of electron cross-field mobility:

$$j_e(x, y) = e \cdot \mu_e(x, y) \cdot n_e(x, y) \cdot E_x(x, y) \quad (23)$$

The sheath width is calculated as Debye layer near the ceramic wall:

$$\lambda_s = \sqrt{\frac{3kT_e \varepsilon_0}{n_e e^2}} \quad (24)$$

The azimuth current J_a will be calculated:

$$j_a(x, y) = e V_a n_e = \frac{eE}{B} \int_0^{\infty} f(V_e) dV \quad (25)$$

where azimuth velocity is the electron drift velocity on crossed electrical and magnetic fields and can be calculated as:

$$V_a = \frac{E(x, y)}{B(x)} \quad (26)$$

F. Boundary conditions and numerical method

The presented model should be supplemented with the following boundary conditions. At the anode plane, we assume the atom density and atom velocity according to equations (1) and (6), with the atom temperature 300 K and atom mass flow rate 3 to 5 mg/s. The input xenon flow is assumed to be uniformly distributed along the channel width. The initial ion temperature near the anode corresponds to ion energy of 3 eV. The external constant electrical field of 100 V/cm was superimposed on the thruster channel between anode plane and exit plane. The channel wall boundary condition consists in wall potential calculated according to equation (22). The wall boundary condition for electron energy equations is the secondary low-energy electron flux from walls to the channel dependent on the primary electron flux to walls and secondary emission coefficient k_s . At the channel exit we specify the electron temperature from 15 eV (at the channel centerline) to 10 eV near the walls, with exponential approximation between these values. The channel was regarded as symmetrical relative to the centerline, i.e. no real curvature of the walls was taken into account.

The system of equations was solved according to the following scheme. Initially the plasma parameters were set using the known potential distribution in the channel. Then the stationary state of electron

component was found for the given plasma parameters. After setting the equilibrium state for the electron fluid component, the ion Vlasov equation was solved. The iteration steps were repeated till the stationary state was achieved. The Poisson equation was solved on each iteration step on the dynamic mesh and extrapolation algorithm that provided significant reduction of the calculation time. The total calculation time amounts to several hours at 2 GHz station.

III. RESULTS AND DISCUSSIONS

The present model was used for computation of the plasma parameters distribution in the Hall thruster channel, with special attention paid to the effect of near wall phenomena on the spatial distribution of calculated values.

A. Plasma parameters in thruster channel

The atom density in channel is shown in Fig. 2 and electron energy distribution along channel is shown in Fig. 3. It can be seen that the density falls from 10^{19} m^{-3} near the anode plane down to less than 10^{18} m^{-3} for the exit. The density change is slow near the anode, and the strongest change is observed near the ionization area, i.e. in the range of 15 to 20 mm of the channel length. In radial direction the atom density increases along entire length of the channel, and the strongest radial change is also observed in the vicinity of the ionization area. For example, at the distance of 20 mm from the anode the atom density increases from $2 \cdot 10^{18} \text{ m}^{-3}$ on the centerline to $5 \cdot 10^{18} \text{ m}^{-3}$ near the wall.

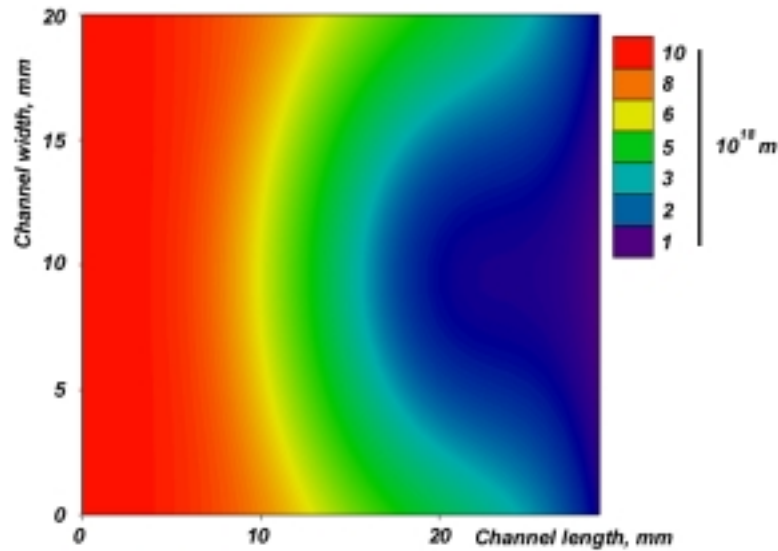


Fig. 2. Atom density distribution in thruster channel.

This pattern of xenon density can be explained taking into account the electron cooling in the vicinity of channel walls. The assumption about the cool secondary electrons emitted by the walls leads to the effective cooling of the electron ensemble in the near-wall region. The ionization cross-section for xenon – electron collisions has a maximum at electron energy of 40 ... 50 eV, and decreases threefold for the energy of 10 eV and less; besides, decrease in electron energy causes decrease in the collision frequency, according to equation (16), where mean electron velocity is used. These effects decrease strongly the rate of xenon ionization, and hence the increase in the xenon density in the near-wall area. In the framework of this model the xenon density cannot be equalized a result of neglecting the atom – atom collisions (2D0V approximation for neutrals).

The mean electron energy along the channel centerline with the secondary emission coefficient k_s as a parameter is shown in Fig. 3. It can be seen that the electron energy rises with k_s decreasing. The maximum values of electron energy are obtained for k_s depending on electron energy. This can be explained in terms of the decrease in electron component cooling by secondary electrons with k_s decreasing. The maximum values of electron energy distribution correspond to the ionization area.

The found regularity can be very important for explaining the fact of anomalous cross-field conductivity in Hall thrusters. As it was mentioned above, two main concepts are used for explaining this phenomenon, namely the concept of near-wall conductivity and concept of Bohm conductivity, which assumes electron scattering on the field fluctuations. The generally accepted point of view for the near-wall conductivity is based on the electron collisions with channel walls. From the above results it can be seen that the elastic electron – atom collision frequency in near-wall region can be increased in several times (thrice at least) and

this can provide the electron mobility comparable with that obtained from the Bohm collisions. Besides, there are two facts important for interpreting the near-wall conductivity phenomena. Firstly, the area of increased xenon density is wide enough (it covers 15% approx. of the channel width from each side, or 30% approx. of the entire channel width). So, it does not cause the pure near-wall conductivity but rather influences the spatial plasma distribution in the channel. Being induced by walls, this process cannot be treated as the near-wall phenomenon, and in this case it is difficult to expect the sine-shaped profile of electron current in channel, as it was predicted theoretically by Morozov^{14,15,16}. Secondly, the near-wall xenon density is mostly increased near the ionization area, where the magnetic field is strong enough and hence the classical mobility is low. Different mechanisms can lead to the same effect of neutral density increase near the wall, such as ion flux neutralization on charged channel walls recently proposed by Ivanov et al¹¹. They show that this effect may significantly enhance the near-wall conductivity in Hall thrusters.

Taking into account the fact that the increased factors are usually used in Bohm collision term (1/50 ... 1/100 as was mentioned above), we can suppose that the fluctuations are small enough for the optimal thruster regimes, and just the increased xenon density due to the wall effect provides the anomalous electron diffusion. Choosing the Bohm factor from the computational results cannot be regarded as methodologically correct approach, and any attempts directed to avoidance this method will be useful.

B. Electron current distribution in thruster channel

The electron current distributions in thruster channel with the secondary electron emission coefficient k_s as a parameter are shown in Figs. 4 – 7, and the currents in thruster exit plane as a function of k_s are shown in Fig. 8. It can be seen that the influence of k_s on the electron current is significant. With higher k_s value, the electron current has mostly convex shape, especially near the anode plane. With lower k_s value, the electron current obtains concave shape, which is formed by increased electron current in the areas located aside of the channel center. The current distribution along the channel length is also affected by the k_s value. For the lower k_s , the electron current distribution along the channel is more convex, as it can be noted by comparing Fig. 4 and Fig. 6: for example, at the length coordinate $X=15$ mm (midpoint of channel length) the relative electron current reaches 0.6 for $k_s=0.75$, and only 0.45 for $k_s=0.95$. The total electron current in exit plane also increased for the case of $k_s=0.75$ and reached 2.8 A (2.2 A for $k_s=0.95$, see Fig. 8).

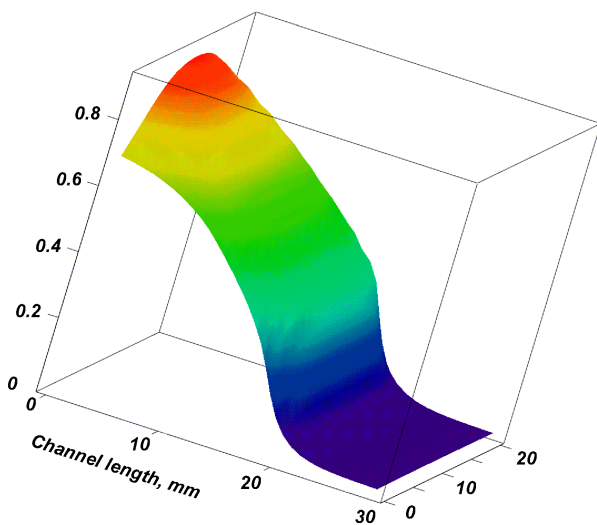


Fig. 4. Normalized electron current distribution in thruster channel. $k_{see} = 0.95$.

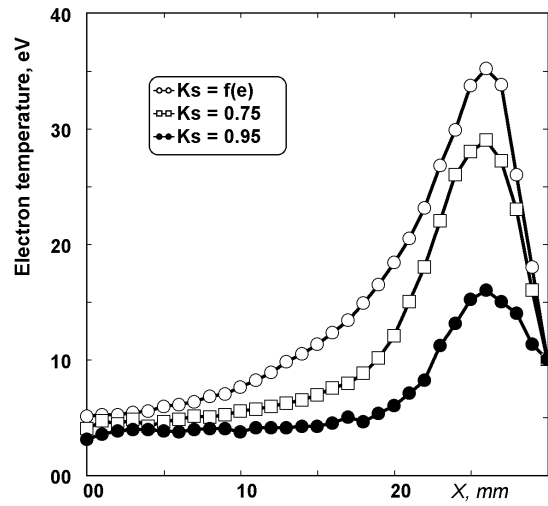


Fig. 3. Electron energy along the channel length with k_s as a parameter.

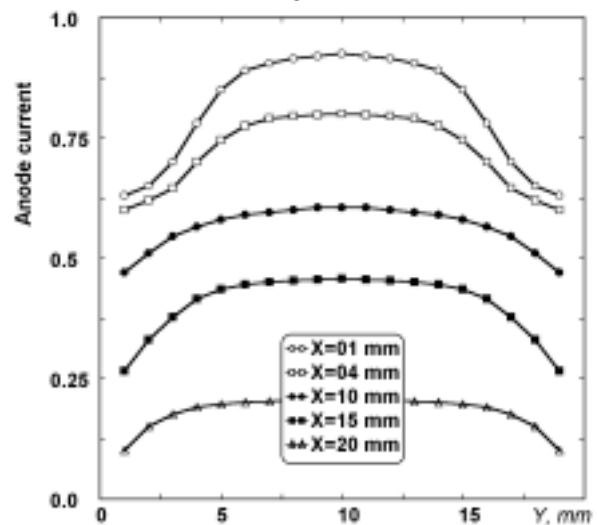


Fig. 5. Normalized electron current profiles across thruster channel. $k_{see} = 0.95$.

Thus, the calculations performed show that the coefficient k_s affects both electron current distribution and total discharge current of thruster, the lower k_s causing increased current and concave current profile near the walls. Both effects can be explained in terms of the physical phenomena involved in the model.

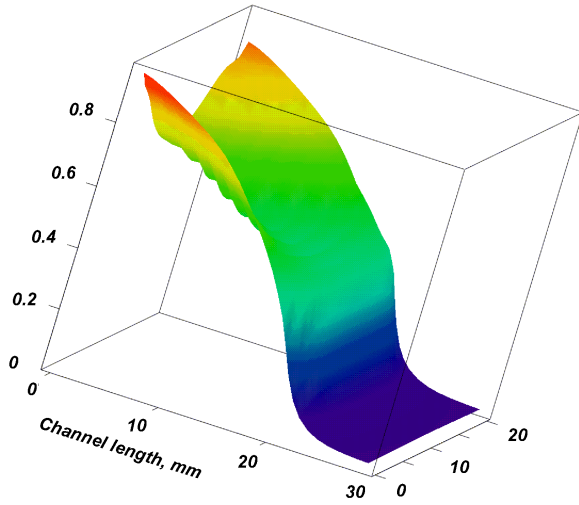


Fig. 6. Normalized electron current distribution in thruster channel. $k_{sec} = 0.75$.

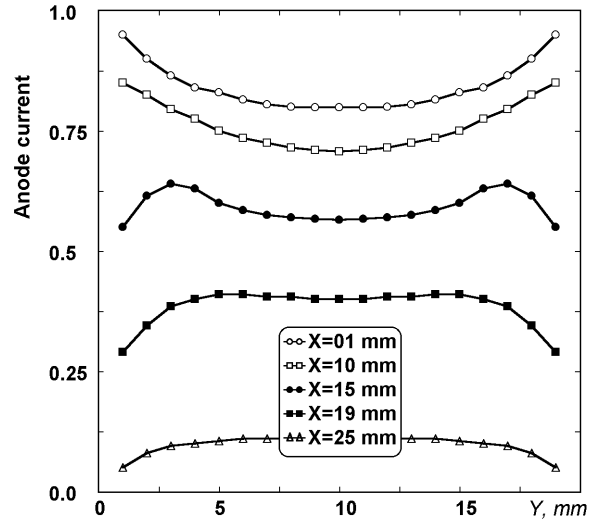


Fig. 7. Normalized electron current profiles across thruster channel. $k_{sec} = 0.75$.

We suppose that these effects are mainly the result of superimposition of two phenomena: cooling of electron ensemble due to the secondary electron emission, and increase of the electron mobility due to the wall collisions (including elastic collisions with xenon atoms in the area of increased density in near-wall area). Let us examine separately the processes that take part in near-exit and near-anode regions of the channel. Near the channel exit (in the ionization area) the magnetic field strength and mean electron energy have the maximum possible values. The secondary electrons emitted from the walls have low energy, they are strongly magnetized in this area and cannot contribute the transversal electron current due to the low collision frequency. However they are repelled from the walls along the magnetic field lines and cool the whole electron ensemble in this area. If we assume that cooling is the main effect of the secondary electron emission, the current increase with for lower k_s is the sound result. Near the anode plane the wall potential is lower. The secondary electrons emitted from the walls cool the electron ensemble temperature mainly near the walls. With high k_s , the near-wall area is intensively cooled due to increased flux of the low-energetic electrons into the near-wall area, and the total mobility in this area decreases. With low k_s , cooling is smaller, and just electron – wall collisions of energetic electrons determine the increased near-wall current. We can suppose that the 'pure' near-wall conductivity stipulated by the electron collisions with wall surface can be found in this area.

C. ION FLUX NEUTRALIZATION ON CHANNEL WALLS

With electron secondary emission coefficient k_s not equal to 1, ceramic walls of the thruster channel will obtain negative potential caused by the electron flux. This effect will produce an ion flux to the walls. This phenomenon was theoretically studied before¹¹. In this work we estimated the influence of the ion flux to the walls and ion flux neutralization on the electrical field distribution in the thruster channel. The flux of the atoms from walls was introduced as atom source on the boundaries equal to the ion flux to the walls. These secondary atoms were used as supplementary component for recalculating atom density.

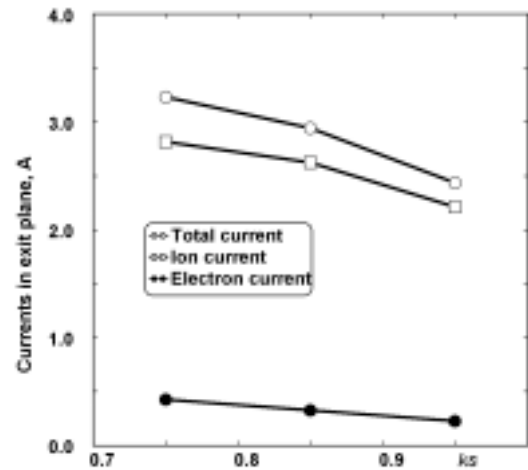


Fig. 8. Total current, ion current and electron current in exit plane as a function of a secondary electron emission coefficient k_s .

The wall potential in this case was calculated as a wall charge balance on the basis of electron flux, secondary electron emission and ion flux to the walls. The previous calculations showed that secondary emission coefficient k_s influences strongly the wall processes in the thruster channel. Taking this into account, we estimated the wall potential for three cases, namely using the boundary values for k_s (0.75 and 0.95), and the equation for k_s as a function of electron energy. According to this approach, the k_s value changes from ≈ 0.5 (for 10 eV) to 0.97 (for 30 eV), i.e. covers the entire range of the emission coefficient used in the similar calculations. It should be noted that the use of above dependence for k_s provides increased wall potentials for the near-wall areas.

The dependencies of ion flux to the thruster walls are shown in Fig. 9. The general shape of the curves (presence of two zero points) can be explained by considering, firstly, the wall potential distribution that tends to zero near the anode, and secondly the high electrical field strength near the thruster exit, which extracts the produced ions quickly from the channel near the exit and prevents them from deposition on the walls. In addition, ion density is rather low near exit, this also provides decrease in the wall flux at this point.

The maximum values of the wall flux do not coincide with the maximum values of wall potential and are located at the midpoint of the channel behind the ionization area. It should be noted that the ionization process is rather intense in this point and the wall potential is relative high. It was natural to suppose that the maximum ion flux to the channel wall should correspond to the maximum wall potential, and the origin of observed disagreement can only be caused by the electrical field re-arrangement. To study this, we have calculated the electrical field in the thruster channel for both cases, i.e. with and without taking into consideration the effect of ion flux neutralization on the channel walls.

The electrical field (absolute magnitude including axial and transversal components) distributions in a channel are shown in Fig. 10 (ion recombination is taken into account) and Fig. 11 (ion recombination is not taken into account). In these calculations we used the k_s dependent on electron energy. It can be seen from these figures that incorporation of the recombination into the model does not affect significantly the maximum value of the electrical field and the location of field peak. It can be explained, as it was mentioned above, by high value of the electrical field in this zone which extracts ions from ionization area and thus eliminates the wall deposition and hence its influence on the location of the ionization area.

Examining the near-wall electrical field distribution, one can see the explicit difference between these two patterns. Examining two typical areas where the patterns are different, namely near-wall area in the ionization zone (close to thruster exit) and near-wall area between channel midpoint and anode plane, we can conclude the following. In the ionization zone (visible in figs. 10 and 11 as the light areas with maximum electrical field), where the electron energy reaches several tenth of eV, the additional atom flow from walls causes intense ionization and the following electron extraction due to the collision – induced mobility. As a result, the low-voltage ions are produced near walls, that decreases both wall potential and the plasma potential in near-wall area, as it can be seen in the Fig. 10.

The spatial (2D) distribution of electron energy in channel being calculated in the model allows to explain this effect by the electron energy change in radial direction. In the near-wall area between channel midpoint and anode plane the electron energy falls down to 10 eV approx., and the ionization is not so intense in this area. The wall potential, nevertheless, is still relatively high in this area due to the appreciable decrease of secondary emission coefficient with the electron energy (we used the k_s dependent on the electron energy for these calculations). The electrons are partly magnetized in this area and transverse mobility is not too high here; as a result, the increased electrical field is maintained in this area. It should be noted that low longitudinal field present in this area (on the channel center) shows that the mean ion energy is very low here and hence the considerable part of the ion flux can be extracted to the walls (not only the slow ions produced in the immediate proximity to the walls). This is apparently the cause of relative high value of the ion flux to the wall in the first part of the channel.

Both noticed effects show that the interaction of ion and electron fluxes with thruster walls plays significant role in the plasma generation and acceleration processes. The study of electron flux interaction is

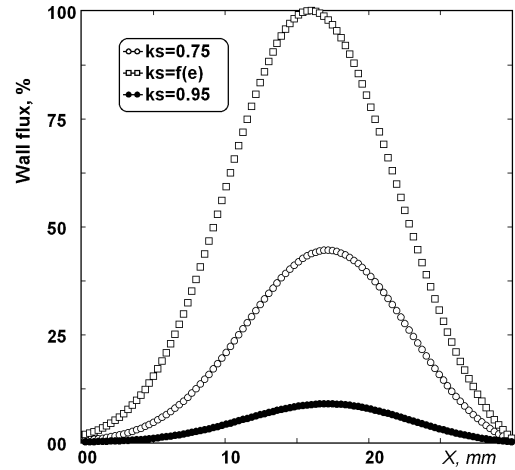


Fig. 9. Ion flux to the channel walls versus channel length with k_s as a parameter.

now widely used for modeling these devices, but the role of ion flux interaction with thruster walls and recombination on the walls should be explored in details.

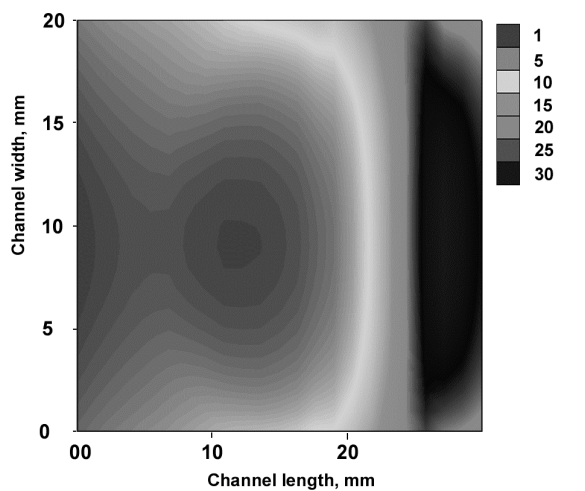


Fig. 10. Electrical field distribution in thruster channel. Ion flux neutralization on channel walls is considered.

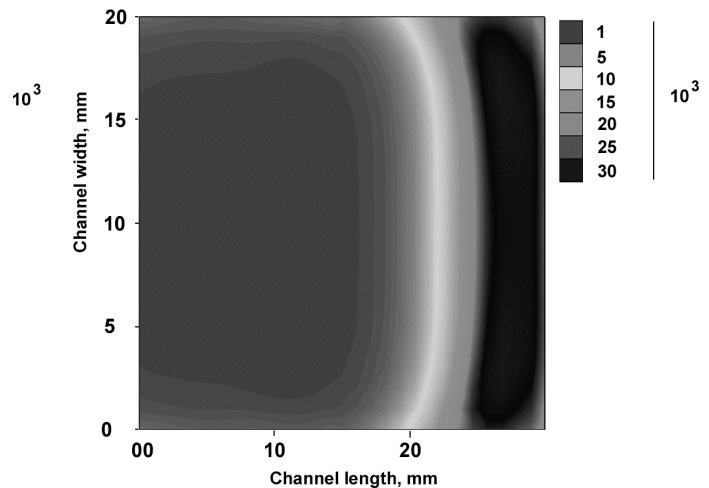


Fig. 11. Electrical field distribution in thruster channel. Ion flux neutralization on channel walls is not considered.

The experimental data on ion fluxes to the walls are not available yet, but we can conclude that in the real thrusters the ion flux to the walls reaches significant value, as it follows from the fact that the significant damage to the ceramic is often observed. It should be mentioned that the damaged zone is mainly located near the thruster exit. We do not see here a contradiction with the found distribution of ion flux along the walls shown in Fig. 9. It is evident that the damage to the ceramic is caused by the high-energetic ions that were deflected gradually in the total electrical field, whereas the main portion of the ion flux to walls consists of the low-energetic ions that were produced in the vicinity on the walls and extracted to the wall surface. Besides, it is natural to assume that some part of the ion flux is produced from the atoms that were recombined before on the walls, because the recombined atom velocity will be uniformly distributed in space and hence they will not leave the near-wall area for some appreciable time.

IV. CONCLUSIONS

We have found that the model developed provides effective modeling of the processes that occur in the plasma of a Hall thruster channel. It was shown that the near-wall processes play the significant role in the thruster physics. The plasma parameters are depend on the secondary emission coefficient and distributed non-uniformly in the thruster channel. The electron-wall collisions, wall potential and ion flux to the walls should be consistently used in the thruster models and can provide the accuracy needed for practical calculations.

Acknowledgments

The authors thank M. Bacal for very useful discussions and comments.

References

- ¹ A.V. Zharinov and Yu.S. Popov, *Sov. Phys. Tech. Phys.* **12**, 208 (1967).
- ² E.Y. Choueiri, *Phys. of Plasmas*, **8**, 11, 5025 (2001).
- ³ G.S. Janes, R.S. Lowder, *Phys. Fluids* **9**, 1115 (1966).
- ⁴ V. V. Zhurin, H. R. Kaufman, and R. S. Robinson, *Plasma Sources Sci. Technol.* **8**, 1 (1999).
- ⁵ A.I. Morozov, *Prikl. Mech. & Tech. Phys.* **3**, 19 (1968).
- ⁶ I. D. Boyd, L. Garrigues, J. Koo, and M. Keidar, *36th AIAA Joint Propulsion Conference, Huntsville, AL, 2000* (AIAA, Washington DC, 2000), AIAA-2000-3520.
- ⁷ J. P. Bouef and L. Garrigues, *J. Appl. Phys.* **84**, 3541 (1998).
- ⁸ M. Keidar, I.D. Boyd, I.I. Beilis, *Phys. of Plasmas*, **8**, 5315 – 5322 (2001).
- ⁹ Y. Raitses, L. Dorf, A. Litvak, N.J. Fisch, *J. Appl. Phys.*, 88 1263 (2000)
- ¹⁰ Y. Raitses, M. Keidar, D. Staack, N.J. Fisch, *J. Appl. Phys.*, 92 4906 (2002)
- ¹¹ A.A. Ivanov, A.A. Ivanov Jr and M. Bacal, *Plasma Phys. and Control. Fusion* **44** (2002) 1463.
- ¹² L. B. King, A. D. Gallimore, and C. M. Marrese, *J. Propul. Power* 14,327 (1998).
- ¹³ V. Yu. Fedotov, A. A. Ivanov, G. Guerrini, A. N. Vesselovzorov, M. Bacal, *Phys. Plasmas*, **6**, 11, 4360 (1999).
- ¹⁴ A. I. Morozov and V. V. Savel'ev, *Plasma Phys. Rep.* **27**, 570 (2001).
- ¹⁵ A. I. Morozov, *Sov. Phys. Dokl.* **10**, 775 (1966).
- ¹⁶ A. I. Morozov and V. V. Savel'ev, *Plasma Phys. Rep.* **26**, 219 (2000).